

Femtosecond X-Ray Diffraction Studies of the Reversal of the Microstructural Effects of Plastic Deformation during Shock Release of Tantalum

M. Sliwa,¹ D. McGonegle,¹ C. Wehrenberg,² C. A. Bolme,³ P. G. Heighway,¹ A. Higginbotham,⁴ A. Lazicki,² H. J. Lee,⁵ B. Nagler,⁵ H. S. Park,² R. E. Rudd,² M. J. Suggit,¹ D. Swift,² F. Tavella,⁵ L. Zepeda-Ruiz,² B. A. Remington,² and J. S. Wark^{1,*}

¹*Department of Physics, Clarendon Laboratory, University of Oxford, Parks Road, Oxford OX1 3PU, United Kingdom*

²*Lawrence Livermore National Laboratory, PO Box 808, Livermore, California 94550, USA*

³*Los Alamos National Laboratory, Bikini Atoll Road, SM-30, Los Alamos, New Mexico 87545, USA*

⁴*York Plasma Institute, Department of Physics, University of York, Heslington, York YO10 5DD, United Kingdom*

⁵*SLAC National Accelerator Laboratory, 2575 Sand Hill Road, Menlo Park, California 94025, USA*



(Received 18 December 2017; published 29 June 2018)

We have used femtosecond x-ray diffraction to study laser-shocked fiber-textured polycrystalline tantalum targets as the 37–253 GPa shock waves break out from the free surface. We extract the time and depth-dependent strain profiles within the Ta target as the rarefaction wave travels back into the bulk of the sample. In agreement with molecular dynamics simulations, the lattice rotation and the twins that are formed under shock compression are observed to be almost fully eliminated by the rarefaction process.

DOI: [10.1103/PhysRevLett.120.265502](https://doi.org/10.1103/PhysRevLett.120.265502)

When a crystal is uniaxially shock compressed to a sufficiently high pressure in the solid phase, beyond the so-called Hugoniot elastic limit, the Hugoniot curve—the locus of states that can be achieved by shock compression—approaches the hydrostat in pressure-volume space, implying that significant plastic deformation has occurred [1]. An understanding of the rapid deformation mechanisms occurring during the shock process at the lattice level, such as the generation and motion of defects, or deformation twinning, has long been sought [2–4]. Of particular interest is the observation that in many cases the high rates of plastic strain observed at the shock front not only cannot be mediated by preexisting dislocations, but are also inconsistent with the defect densities found after the event. That is to say a direct application of Orowan's equation [5], $\dot{\epsilon}_p = \rho |\mathbf{b}| v$, where $\dot{\epsilon}_p$ is the plastic strain rate, ρ the number of mobile dislocations per unit area with Burgers vector \mathbf{b} and velocity v , implies (under the assumption of subsonic dislocations) dislocation densities behind the shock front that can be several orders of magnitude greater than both those initially present, and those found in recovered samples.

While defect densities consistent with observed plastic strain rates are not found in recovered samples [6,7], such high densities are observed in many molecular dynamics (MD) simulations [8,9], and long prior to those simulations the generation of high densities of homogeneously nucleated dislocations at the shock front had been proposed [3]. A resolution to this discrepancy is suggested by further MD simulations that show that upon the shock unloading at a free surface, and subsequent rarefaction, most of the dislocations annihilate [10] implying that analysis of recovered samples may at best not provide a full picture

of the conditions present during the passage of the shock itself. The large defect densities thought to be present under shock compression may also be pertinent to apparent contradictions in measured melting temperatures at high pressure [11–13]. Common methods of interrogating sample response, such as velocimetry techniques using VISAR (velocity interferometer system for any reflector) [14], rely on measurements of the velocity of the free surface in order to deduce the sample's response [15]. However, this kind of method provides a limited amount of information since it does not probe either the plastic behavior at the lattice level or the state of the entirety of the material at one particular moment. It thus cannot be used to address the above hypothesis that microstructural plastic deformation during the shock can be, at least to some extent, eliminated upon release.

It is within the context outlined above that we present the results of experiments where, via femtosecond x-ray diffraction (XRD), we directly observe the microstructural effects of shock-induced plasticity being reversed in polycrystalline tantalum during shock breakout as the rarefaction wave travels back into the sample (although overall entropy increase, evinced by shock heating, would still be irreversible). In particular, we directly observe the reduction of shock-induced twins as well as a significant reversal in the lattice rotation imparted during the shock-compression process. These results, which are in good agreement with MD simulations, provide conclusive evidence that the release of stress after shock events, and the associated subsequent rarefactions and reverberations, can significantly alter the microstructure of the sample from that

extant during the shock itself, highlighting the importance of *in situ* measurements.

Shock-induced plasticity in tantalum, a body-centered cubic metal, has been studied extensively, with analyses of recovered samples [6,16–19] being complemented by a number of MD studies [9,20–23]. Here we use XRD to directly monitor lattice orientations during shock release. The technique of *in situ* XRD to study shock-compressed materials has been developed over several years utilizing a number of different shock drivers and x-ray sources, including diodes [24–27], laser-produced-plasmas [28–33] and third generation synchrotrons [34–37]. More recently, with the advent of fourth generation light sources such as the Linac Coherent Light Source (LCLS), single-shot 100 fs diffraction patterns can be obtained from laser-shocked crystals, providing lattice-level information on a timescale shorter than even the fastest phonon period [38–43].

The experiment was performed at the Matter in Extreme Conditions (MEC) endstation of LCLS [44]. A schematic diagram of the experimental setup is shown in Fig. 1. The targets comprised a 50- μm -thick polyimide ablator glued to a 6- μm -thick foil of polycrystalline Ta with a fiber texture such that the majority of the crystallites were oriented with their [110] axes parallel, within a few degrees, to the normal to the target surface, but azimuthally around these axes the grains were oriented approximately randomly (a pole plot is shown in the Supplemental Material [45]). As explained in more detail below, such a texture allows direct monitoring of lattice rotation and twinning via XRD. A 5 ns, flat-topped, frequency doubled (527 nm) laser pulse was used

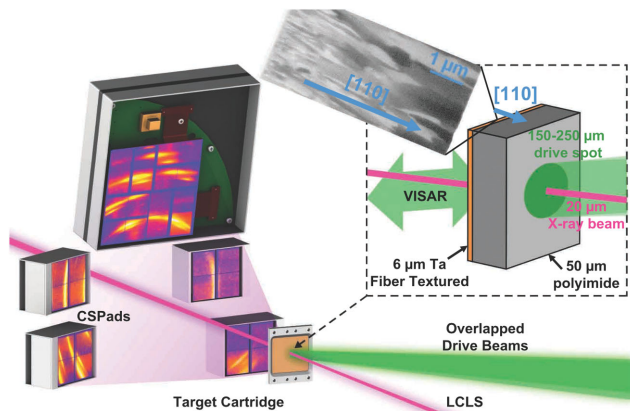


FIG. 1. A schematic diagram of the experimental setup. The fiber-textured Ta sample is shocked along the crystallographic [110] direction via laser ablation of the polyimide overcoat. A SEM micrograph of the Ta sample (inset) shows the columnar microstructure that gives rise to the fiber texture. The driven material is probed with x rays that are incident at an angle of 35° to the surface normal, and diffraction images are collected on an array of CSPADs. A VISAR system interrogates the rear surface velocity of the sample. Figure adapted from Wehrenberg *et al.* [43].

to drive a shock into the target. By varying the intensity of the drive laser it was possible to obtain shock pressures of 37 ± 2 to 253 ± 6 GPa, as measured via the position of the Bragg peaks considering volumetric compression of the crystal lattice together with the Rankine-Hugoniot equations using the shock speed data [46]. The LCLS beam (9.6 keV, 50 fs duration) probed the compressed region after a set delay (from just before to ~ 10 ns after shock break out) and the resulting diffraction patterns were captured on a number of Cornell-SLAC Pixel Array Detectors (CSPADs) [47]. The target was oriented such that the surface normal was aligned at an angle of 35° to the x-ray beam.

By bringing the x-ray beam in at an angle to the compression axis of the fiber-textured target we are able to directly monitor lattice rotation and twinning. Such a geometry does not produce full Debye-Scherrer (DS) rings, but distinct arcs on each ring, the azimuthal position of which provides direct information on the orientation of the planes with respect to the shock direction, [48] and which previously enabled the observation of lattice rotation due to slip and twinning under shock compression [43]. The texture direction is aligned with the sample's normal, and we define angles χ between the sample's normal and the normals to the lattice planes producing the diffraction spots, and denote by χ_0 such angles for the ambient unshocked material.

The shock wave is characterized by a high-strain rate resulting in a sharp discontinuity in the strain at the shock front. Therefore, during the passage of the shock before it reaches the rear free surface, diffraction from both compressed and ambient material is observed, resulting in arcs lying on two distinct well-defined DS rings, with negligible diffraction signal between them, as shown in Fig. 2(a). When the shock encounters the free surface, the normal

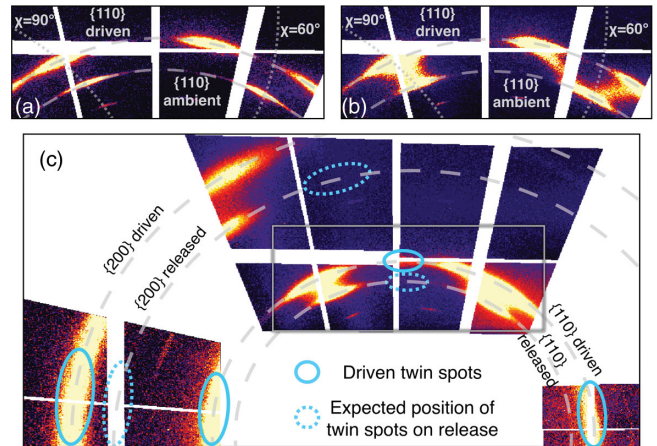


FIG. 2. XRD images of Ta during (a) the initial shock passage at 167 GPa, (b) release following 150 GPa, and (c) 75 GPa shocks. In (c) diffraction due to twins is marked with full circles, and the positions of the expected locations of twin spots on release are marked with dashed circles. Images (a) and (b) correspond to the CSPADs' coverage marked with the full rectangle encompassing (c).

component of the stress at that surface must remain zero, so a rarefaction wave is launched back into the sample allowing material to expand quasi-isentropically [49]. In contrast to the extremely rapid change of strain at the shock front, a rarefaction fan ensues owing to the reduction in the local speed of sound as the pressure drops, leading to a release of strain at a decreasing rate as the rarefaction proceeds. This much lower strain gradient exhibits itself as a clear diffraction signal over the whole range of Bragg angles between those DS rings that correspond to fully compressed and fully released material, as shown in Fig. 2(b). As we show below, the distribution of diffracted intensity in this region allows us to extract the instantaneous strain-depth profiles in the rarefaction fan.

Several important observations can be made immediately from the data. As has been shown in Ref. [43] under [110] compression in these samples, the shock-induced shear stress is relieved by either slip on the $\{112\}\langle 111\rangle$ system or $\{112\}$ twinning. Since the material is laterally confined, in order to preserve the geometry of uniaxial compression, both slip and twinning induce crystal lattice rotations [31,43,50] about $[1\bar{1}0]$ which can be directly related to the amount of shear stress relieved.

Lattice rotation can be measured from the azimuthal position of the diffraction. For example, for the (110) ring, the diffraction peak at $\chi_0 = 90^\circ$ preserves its azimuthal position upon compression as grains diffracting in this orientation have their (110) planes with normals perpendicular to the shock propagation direction. However, the diffraction at $\chi_0 \neq 90^\circ$ splits under compression since the corresponding diffraction planes rotate towards and away from the compression axis. Figure 2(a) shows an example of lattice rotations inferred from the (110) Bragg reflections for a shock pressure of 150 GPa, where the diffraction signal on the left follows the $\chi_0 = 90^\circ$ path while the $\chi_0 = 60^\circ$ diffraction signal splits on compression into $\chi > 60^\circ$ and $\chi < 60^\circ$, and the magnitude of the splitting implies a lattice rotation of just over 10° in the shocked state. On release we observe diffraction along paths connecting the diffraction signal from the fully-compressed and fully-released material at the rear surface, which provides an explicit *in situ* history of lattice rotations during rarefaction. As shown in Fig. 2(b), the diffraction signal traces out a path along the $\chi = 90^\circ$ line, while the $\chi = 60^\circ$ signal, split during compression, traces paths back close to its initial position. This is indicative of reversed lattice rotations on release about $[1\bar{1}0]$. Reversed lattice rotations, even though not explicitly confirming dislocation annihilation, suggest inverted dislocation motion. It should be noted that a small residual azimuthal split between peaks which were originally at $\chi_0 = 60^\circ$ in the ambient sample is observed, corresponding to residual lattice rotations up to $\sim 3^\circ$ in magnitude, compared with the rotation of $\sim 10^\circ$ in the shocked state.

As well as the observation of a shock-induced splitting of those spots with $\chi_0 \neq 90^\circ$, we also observe the appearance

of a completely new set of $\chi \neq 90^\circ$ diffraction spots corresponding to the formation of twins. The relative intensity of these spots provides a measure of the degree of twinning within the sample, which has been found to maximize at a volume fraction of order 30% between shock pressures of 50 and 150 GPa [43]. Figure 2(c) shows a diffraction pattern during release after a passage of 75 GPa shock, which on compression generates large amounts of twinning, with the diffraction associated with the twins marked both under compression, and where they would be expected to appear under release. It can be seen that no signal corresponding to twins is observed in the released state, indicating disappearance upon rarefaction (to a fraction below 1%, a figure determined by the noise background).

This experimental observation of detwinning, supported by MD simulations below, is interesting in the context of previous studies of recovered materials. Contrary to the monocrystalline [17–19] and polycrystalline [16] samples which show significant amounts of twinning remaining after the shock, nanocrystalline materials [6] have not shown traces of twins. This phenomenon has been considered in terms of the Hall-Petch effect which suggests that large grains twin more easily. However, the evidence of detwinning in the high-strain-rate experiment brings a new perspective on those studies. Furthermore, twinning-detwinning deformation in grains with transverse dimensions of the order of 100 nm (see micrograph in Fig. 1) may be analogous to the cyclic loading-unloading experiments performed on nanopillars [51], suggesting pseudoelastic properties of the nanoscale materials not only on the static, but also on the dynamic timescales.

In order to complement these observations of the partial reversal of lattice rotation and detwinning upon release we have performed MD simulations using the LAMMPS code [52]. Using the Ravelo EAM Ta1 potential [22], we simulated the response of a $100 \times 100 \times 950$ cells ($33 \times 33 \times 314$ nm) Ta single crystal at 300 K to a moving piston along the [110] direction, with periodic boundaries in the transverse directions. Piston velocities in the range $0.7\text{--}1.2$ km s $^{-1}$ were applied which drove shocks of strengths between 50–100 GPa. The simulation time was sufficiently long that we could observe both shock propagation and subsequent rarefaction from the rear surface. Upon release (which occurs just before 70 ps in the simulations), the shear stress changes its sign with respect to the one observed during initial shock passage as shown in Fig. 3(a) for a shock of 100 GPa. As a result, it causes a significant reversal of the microstructural plastic deformation induced by the shock, in good agreement with our experimental findings. Using a nearest neighbor analysis we identified variations in lattice orientation across the sample. Figure 3(b) presents the average lattice rotation about the $[1\bar{1}0]$ direction as a function of longitudinal position within the sample at different times. In agreement with the experiment, it can be observed that the simulated

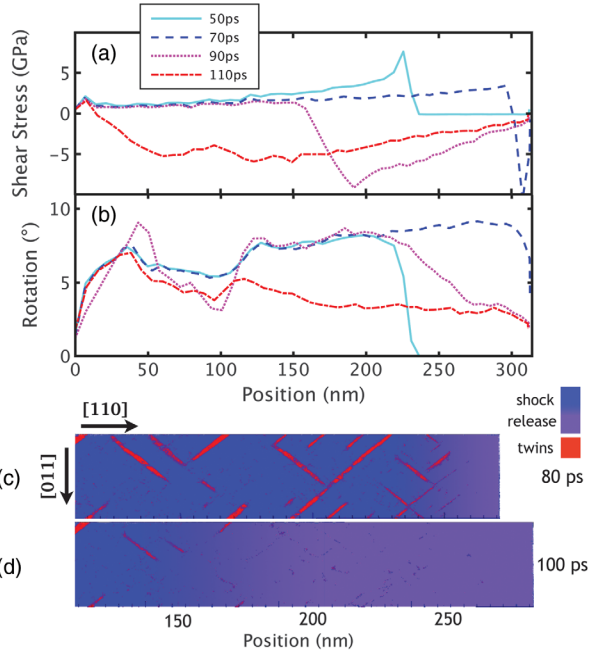


FIG. 3. Average rotation angle about $[1\bar{1}0]$ direction (a) and shear stress defined as $(\sigma_{zz} - \sigma_{xx})/2$ (b) along the Lagrangian position in a single crystal Ta as a function of time in MD simulation with 100 GPa shock moving to the right and the rarefaction wave propagating to the left (after 70 ps). (c) and (d) show the visualizations in Eulerian coordinates of the regions rotated by more than 20° at the time steps 80 ps and 100 ps for the case of 50 GPa shock. This method allows for an easy observation of the twinned parts (thick, red well-defined lines). Blue and purple regions correspond to the nontwinned shocked and released parts of the sample, respectively.

sample experiences reversed lattice rotations as a result of rarefaction. The quantitative rotations are in excellent agreement with the experiment, where we also see a maximum rotation of the lattice of order 8° at 100 GPa. Furthermore, the simulations also indicate that upon rarefaction not all of the rotation is reversed, with a residual rotation of approximately 3° persisting in the simulation. Using a dislocation extraction analysis [53,54] we also find a reduction of a factor of 2.5 of the dislocation density upon rarefaction from a peak value of $5 \times 10^{13} \text{ cm}^{-2}$ behind the shock. In addition, as can be seen Fig. 3(c) the MD simulations with a 50 GPa shock predict significant twinning (a twin fraction of 6%) upon compression, but in agreement with the experiment, and as can be seen in Fig. 3(d), the twins disappear upon release.

The experimental data allow us to extract the strain transverse to shock propagation direction as a function of depth. The strength of the diffraction signal at a particular angle between that corresponding to the totally released material, and that still under peak compression, is a measure of the amount of material at a given strain. As shown in the Supplemental Material [45], this allows us to iteratively construct a transverse $[1\bar{1}0]$ strain profile (for this

direction the elastic component of the strain, to which diffraction is sensitive, is equal and opposite to the plastic strain) that is consistent with the diffraction image, under the assumption that the strain within the sample varies monotonically. Such algorithms have been used previously to deduce strain profiles from diffraction profiles [55,56].

The deduced strain profiles as a function of depth and time are shown in Fig. 4(a). As expected, the strain gradient becomes shallower as the rarefaction proceeds. Indeed, we can construct a model of the propagation of the release wave showing that the rate of reduction of the strain gradient is consistent with a simple model (see Supplemental Material [45], which includes Refs. [57,58]). Given that the elastic strain that we measure is that transverse to the shock direction, and thus insensitive to any purely elastic longitudinal release, we approximate the strain gradient, α , within the rarefaction fan as a function of the position of the release tail, z :

$$\alpha = \frac{\epsilon C_0}{[C_B(1 - \epsilon)^{-3} - C_0]z}, \quad (1)$$

where C_B and C_0 are the bulk sound speeds at the shock pressure and ambient conditions, respectively, and ϵ is the plastic strain in the shocked region.

Figure 4(b) shows the evolution of the strain gradient extracted from the data as a function of time, as well as analytic values from Eq. (1) and the prediction of the 1D hydrodynamic (HYADES [59]) and the MD simulations. Good agreement has been found between the first three methods. The slightly lower than predicted experimental inverse strain gradient at $3.7 \mu\text{m}$ is due to the onset of release on the front (driven) side of the Ta foil. By using

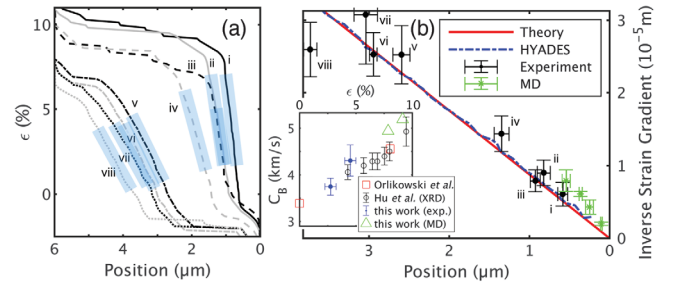


FIG. 4. (a) Extracted transverse strain profiles from the XRD images as a function of Lagrangian position of the sample along the shocked direction with $0 \mu\text{m}$ and $6 \mu\text{m}$ referring to the back surface and the polyimide/Ta interface, respectively. Selected profiles correspond to samples driven by shocks of 50–100 GPa. (b) Inverse strain gradient [from the shaded regions in (a)] as a function of the position of the tail of release wave front (taken at $\epsilon = 0$). A theoretical prediction (red line), HYADES (blue dashed line), and MD (green asterisks), obtained for the case of 100 GPa shock, are also shown. The inset shows inferred bulk sound speed as a function of transverse elastic strain, and compares this with previous data assuming hydrostatic response.

Eq. (1), for $C_0 = 3293 \text{ ms}^{-1}$ [46], the bulk sound speed in the shocked state can be estimated. While the MD simulations predict slightly lower strain gradients than those seen experimentally, the finite size of the simulations means that significant elastic-plastic kinetics may still be occurring during the simulation time, and consequently the MD implies slightly larger sound speeds than suggested by the XRD measurement and previous studies [60,61]. Furthermore, the effects of finite shear strain within the rarefaction fan itself are not taken into account in this simple model, and this may also affect the accuracy of any deduced sound speeds. What is clear, however, is that the rate of reduction of the strain gradient deduced from the diffraction signals is consistent with that expected.

In conclusion, we have performed *in situ* femtosecond XRD studies of the release of shocked fiber-textured polycrystalline tantalum. We observe that the significant lattice rotations imparted by the shock are largely reversed upon shock breakout as the rarefaction wave travels back into the sample. We also observe a complete reversal of the shock-induced twinning. The experimental data are in good agreement with MD simulations, and this direct observation of the reversal of microstructural changes upon release emphasizes the important contribution that such *in situ* studies can make to our understanding of the physics of shock deformation at the lattice level. Indeed, while this work was in the proof stage, we learnt of recent similar types of measurements in shocked magnesium crystals [62].

J. S. W. is grateful to the UK EPSRC for support under Grant No. EP/J017256/1. M. S. and D. M. were supported by LLNS under Contracts No. B609694 and No. B595954, respectively. Use of the Linac Coherent Light Source (LCLS), SLAC National Accelerator Laboratory, is supported by the U.S. Department of Energy, Office of Science, Office of Basic Energy Sciences under Contract No. DE-AC02-76SF00515. The MEC instrument is supported by the U.S. Department of Energy, Office of Science, Office of Fusion Energy Sciences under Contract No. SF00515. This material is based upon work supported by the U.S. Department of Energy, Office of Science, Office of Fusion Energy Sciences, under Award No. DE-SCW-1507. This work was performed in part under the auspices of the U.S. Department of Energy by Lawrence Livermore National Laboratory under Contract No. DE-AC52-07NA27344.

*justin.wark@physics.ox.ac.uk

- [1] J. W. Taylor, *J. Appl. Phys.* **36**, 3146 (1965).
- [2] C. S. Smith, *Trans. Metall. Soc. AIME* **212**, 574 (1958).
- [3] M. A. Meyers, *Scr. Metall.* **12**, 21 (1978).
- [4] F. A. Bandak, R. W. Armstrong, and A. S. Douglas, *Phys. Rev. B* **46**, 3228 (1992).
- [5] E. Orowan, *Proc. Phys. Soc. London* **52**, 8 (1940).
- [6] C. H. Lu, B. A. Remington, B. R. Maddox, B. Kad, H. S. Park, M. Kawasaki, T. G. Langdon, and M. A. Meyers, *Acta Mater.* **61**, 7767 (2013).
- [7] L. L. Hsiung, *J. Phys. Condens. Matter* **22**, 385702 (2010).
- [8] E. M. Bringa, K. Rosolankova, R. E. Rudd, B. A. Remington, J. S. Wark, M. Duchaineau, D. H. Kalantar, J. Hawreliak, and J. Belak, *Nat. Mater.* **5**, 805 (2006).
- [9] D. Tramontina, P. Erhart, T. Germann, J. Hawreliak, A. Higginbotham, N. Park, R. Ravelo, A. Stukowski, M. Suggit, Y. Tang, J. Wark, and E. Bringa, *High Energy Density Phys.* **10**, 9 (2014).
- [10] H. N. Jarmakani, E. M. Bringa, P. Erhart, B. A. Remington, Y. M. Wang, N. Q. Vo, and M. A. Meyers, *Acta Mater.* **56**, 5584 (2008).
- [11] D. Errandonea, M. Somayazulu, D. Husermann, and H. K. Mao, *J. Phys. Condens. Matter* **15**, 7635 (2003).
- [12] C. J. Wu, P. Söderlind, J. N. Glosli, and J. E. Klepeis, *Nat. Mater.* **8**, 223 (2009).
- [13] J. Ruiz-Fuertes, A. Karandikar, R. Boehler, and D. Errandonea, *Phys. Earth Planet. Inter.* **181**, 69 (2010).
- [14] P. M. Celliers, D. K. Bradley, G. W. Collins, D. G. Hicks, T. R. Boehly, and W. J. Armstrong, *Rev. Sci. Instrum.* **75**, 4916 (2004).
- [15] P. A. Rigg, R. J. Scharff, and R. S. Hixson, *J. Phys. Conf. Ser.* **500**, 032018 (2014).
- [16] L. E. Murr, M. A. Meyers, C.-S. Niou, Y. J. Chen, S. Pappu, and C. Kennedy, *Acta Mater.* **45**, 157 (1997).
- [17] L. M. Hsiung and D. H. Lassila, *Acta Mater.* **48**, 4851 (2000).
- [18] C. H. Lu, C. H. Remington, B. R. Maddox, B. Kad, H. S. Park, S. T. Prisbrey, and M. A. Meyers, *Acta Mater.* **60**, 6601 (2012).
- [19] J. N. Florando, N. R. Barton, B. S. El-Dasher, J. M. McNaney, and M. Kumar, *J. Appl. Phys.* **113**, 083522 (2013).
- [20] R. E. Rudd, A. J. Comley, J. Hawreliak, B. R. Maddox, H. S. Park, and B. A. Remington, *AIP Conf. Proc.* **1426**, 1379 (2012).
- [21] A. Higginbotham, M. J. Suggit, E. M. Bringa, P. Erhart, J. A. Hawreliak, G. Mogni, N. Park, B. A. Remington, and J. S. Wark, *Phys. Rev. B* **88**, 104105 (2013).
- [22] R. Ravelo, T. C. Germann, O. Guerrero, Q. An, and B. L. Holian, *Phys. Rev. B* **88**, 134101 (2013).
- [23] D. R. Tramontina, E. N. Hahn, M. A. Meyers, and E. M. Bringa, *AIP Conf. Proc.* **1793**, 070002 (2017).
- [24] Q. Johnson, A. Mitchell, R. N. Keeler, and L. Evans, *Phys. Rev. Lett.* **25**, 1099 (1970).
- [25] Q. Johnson, A. Mitchell, and L. Evans, *Nature (London)* **231**, 310 (1971).
- [26] Q. Johnson and A. C. Mitchell, *Phys. Rev. Lett.* **29**, 1369 (1972).
- [27] Q. Johnson, A. C. Mitchell, and L. Evans, *Appl. Phys. Lett.* **21**, 29 (1972).
- [28] J. S. Wark, R. R. Whitlock, A. Hauer, J. E. Swain, and P. J. Solone, *Phys. Rev. B* **35**, 9391 (1987).
- [29] J. S. Wark, R. R. Whitlock, A. A. Hauer, J. E. Swain, and P. J. Solone, *Phys. Rev. B* **40**, 5705 (1989).
- [30] A. Loveridge-Smith, A. Allen, J. Belak, T. Boehly, A. Hauer, B. Holian, D. Kalantar, G. Kyralla, R. W. Lee, P. Lomdahl, M. A. Meyers, D. Paisley, S. Pollaine, B. Remington, D. C. Swift, S. Weber, and J. S. Wark, *Phys. Rev. Lett.* **86**, 2349 (2001).

- [31] M. J. Suggit, A. Higginbotham, J. A. Hawreliak, G. Mogni, G. Kimminau, P. Dunne, A. J. Comley, N. Park, B. A. Remington, and J. S. Wark, *Nat. Commun.* **3**, 1224 (2012).
- [32] A. J. Comley, B. R. Maddox, R. E. Rudd, S. T. Prsbrey, J. A. Hawreliak, D. A. Orlikowski, S. C. Peterson, J. H. Satcher, A. J. Elsholz, H. S. Park, B. A. Remington, N. Bazin, J. M. Foster, P. Graham, N. Park, P. A. Rosen, S. R. Rothman, A. Higginbotham, M. Suggit, and J. S. Wark, *Phys. Rev. Lett.* **110**, 115501 (2013).
- [33] C. E. Wehrenberg, A. J. Comley, N. R. Barton, F. Coppari, D. Fratanduono, C. M. Huntington, B. R. Maddox, H. S. Park, C. Plechaty, S. T. Prsbrey, B. A. Remington, and R. E. Rudd, *Phys. Rev. B* **92**, 104305 (2015).
- [34] S. J. Turneaure, Y. M. Gupta, K. Zimmerman, K. Perkins, C. S. Yoo, and G. Shen, *J. Appl. Phys.* **105**, 053520 (2009).
- [35] S. J. Turneaure and Y. M. Gupta, *J. Appl. Phys.* **106**, 033513 (2009).
- [36] Y. M. Gupta, S. J. Turneaure, K. Perkins, K. Zimmerman, N. Arganbright, G. Shen, and P. Chow, *Rev. Sci. Instrum.* **83**, 123905 (2012).
- [37] S. J. Turneaure, N. Sinclair, and Y. M. Gupta, *Phys. Rev. Lett.* **117**, 045502 (2016).
- [38] D. Milathianaki, S. Boutet, G. J. Williams, A. Higginbotham, D. Ratner, A. E. Gleason, M. Messerschmidt, M. M. Seibert, D. C. Swift, P. Hering, J. Robinson, W. E. White, and J. S. Wark, *Science* **342**, 220 (2013).
- [39] M. G. Gorman, R. Briggs, E. E. McBride, A. Higginbotham, B. Arnold, J. H. Eggert, D. E. Fratanduono, E. Galtier, A. E. Lazicki, H. J. Lee, H. P. Liermann, B. Nagler, A. Rothkirch, R. F. Smith, D. C. Swift, G. W. Collins, J. S. Wark, and M. I. McMahon, *Phys. Rev. Lett.* **115**, 095701 (2015).
- [40] A. E. Gleason, C. A. Bolme, H. J. Lee, B. Nagler, E. Galtier, D. Milathianaki, J. Hawreliak, R. G. Kraus, J. H. Eggert, D. E. Fratanduono, G. W. Collins, R. Sandberg, W. Yang, and W. L. Mao, *Nat. Commun.* **6**, 8191 (2015).
- [41] R. Briggs, M. G. Gorman, A. L. Coleman, R. S. McWilliams, E. E. McBride, D. McGonegle, J. S. Wark, L. Peacock, S. Rothman, S. G. Macleod, C. A. Bolme, A. E. Gleason, G. W. Collins, J. H. Eggert, D. E. Fratanduono, R. F. Smith, E. Galtier, E. Granados, H. J. Lee, B. Nagler *et al.*, *Phys. Rev. Lett.* **118**, 025501 (2017).
- [42] A. E. Gleason, C. A. Bolme, E. Galtier, H. J. Lee, E. Granados, D. H. Dolan, C. T. Seagle, T. Ao, S. Ali, A. Lazicki, D. Swift, P. Celliers, and W. L. Mao, *Phys. Rev. Lett.* **119**, 025701 (2017).
- [43] C. E. Wehrenberg, D. McGonegle, C. Bolme, A. Higginbotham, A. Lazicki, H. J. Lee, B. Nagler, H.-S. Park, B. A. Remington, R. E. Rudd, M. Sliwa, M. Suggit, D. Swift, F. Tavella, L. Zepeda-Ruiz, and J. S. Wark, *Nature (London)* **550**, 496 (2017).
- [44] B. Nagler, B. Arnold, G. Bouchard, R. F. Boyce, R. M. Boyce, A. Callen, M. Campbell, R. Curiel, E. Galtier, J. Garofoli, E. Granados, J. Hastings, G. Hays, P. Heimann, R. W. Lee, D. Milathianaki, L. Plummer, A. Schropp, A. Wallace, M. Welch *et al.*, *J. Synchrotron Radiat.* **22**, 520 (2015).
- [45] See Supplemental Material at <http://link.aps.org/supplemental/10.1103/PhysRevLett.120.265502> for more details concerning target fabrication, strain profile extraction, and release modeling.
- [46] A. C. Mitchell and W. J. Nellis, *J. Appl. Phys.* **52**, 3363 (1981).
- [47] H. T. Philipp, M. Hromalik, M. Tate, L. Koerner, and S. M. Gruner, *Nucl. Instrum. Methods Phys. Res., Sect. A* **649**, 67 (2011).
- [48] D. McGonegle, D. Milathianaki, B. A. Remington, J. S. Wark, and A. Higginbotham, *J. Appl. Phys.* **118**, 065902 (2015).
- [49] M. A. Meyers, *Dynamic Behaviour of Materials* (John Wiley and Sons, Inc., New York, 1994).
- [50] R. L. Fleischer, *J. Mech. Phys. Solids* **6**, 301 (1958).
- [51] J. Wang, Z. Zeng, C. R. Weinberger, Z. Zhang, T. Zhu, and S. X. Mao, *Nat. Mater.* **14**, 594 (2015).
- [52] S. Plimpton, *J. Comput. Phys.* **117**, 1 (1995).
- [53] A. Stukowski, *Model. Simul. Mater. Sci. Eng.* **18**, 015012 (2010).
- [54] A. Stukowski and K. Albe, *Model. Simul. Mater. Sci. Eng.* **18**, 085001 (2010).
- [55] B. C. Larson, C. W. White, T. S. Noggle, J. F. Barhorst, and D. M. Mills, *Appl. Phys. Lett.* **42**, 282 (1983).
- [56] C. Rose-Petruck, R. Jimenez, T. Guo, A. Cavalleri, C. W. Siders, F. Rksi, J. A. Squier, B. C. Walker, K. R. Wilson, and C. P. J. Barty, *Nature (London)* **398**, 310 (1999).
- [57] J. M. Walsh, M. H. Rice, R. G. McQueen, and F. L. Yarger, *Phys. Rev.* **108**, 196 (1957).
- [58] R. G. McQueen, J. W. Hopson, and J. N. Fritz, *Rev. Sci. Instrum.* **53**, 245 (1982).
- [59] J. T. Larsen and S. M. Lane, *J. Quant. Spectrosc. Radiat. Transfer* **51**, 179 (1994).
- [60] D. Orlikowski, P. Söderlind, and J. A. Moriarty, *Phys. Rev. B* **74**, 054109 (2006).
- [61] J. Hu, C. Dai, Y. Yu, Z. Liu, Y. Tan, X. Zhou, H. Tan, L. Cai, and Q. Wu, *J. Appl. Phys.* **111**, 033511 (2012).
- [62] S. J. Turneaure, P. Renganathan, J. M. Winey, and Y. M. Gupta, following Letter, *Phys. Rev. Lett.* **120**, 265503 (2018).